Microsc. Microanal., page 1 of 8
doi:10.1017/S1431927614000464

Microscopy AND Microanalysis



# *In Situ* Observation of Electron Beam-Induced Phase Transformation of $CaCO_3$ to CaO via ELNES at Low Electron Beam Energies

Ute Golla-Schindler,[1,*] Gerd Benner,[2] Alexander Orchowski,[2] and Ute Kaiser[1]

[1]*Group of Electron Microscopy of Material Science, University Ulm, Albert-Einstein-Allee 11, 89081 Ulm, Germany*
[2]*Materials Division, Carl Zeiss Microscopy GmbH, Carl-Zeiss Str. 22, 73447 Oberkochen, Germany*

**Abstract:** It is demonstrated that energy-filtered transmission electron microscope enables following of *in situ* changes of the Ca-$L_{2,3}$ edge which can originate from variations in both local symmetry and bond lengths. Low accelerating voltages of 20 and 40 kV slow down radiation damage effects and enable study of the start and finish of phase transformations. We observed electron beam-induced phase transformation of single crystalline calcite ($CaCO_3$) to polycrystalline calcium oxide (CaO) which occurs in different stages. The coordination of Ca in calcite is close to an octahedral one streched along the $< 111 >$ direction. Changes during phase transformation to an octahedral coordination of Ca in CaO go along with a bond length increase by 5 pm, where oxygen is preserved as a binding partner. Electron loss near-edge structure of the Ca-$L_{2,3}$ edge show four separated peaks, which all shift toward lower energies during phase transformation at the same time the energy level splitting increases. We suggest that these changes can be mainly addressed to the change of the bond length on the order of picometers. An important pre-condition for such studies is stability of the energy drift in the range of meV over at least 1 h, which is achieved with the sub-Ångström low-voltage transmission electron microscope I prototype microscope.

**Key words:** ELNES, low kV TEM, SALVE, $CaCO_3$ (calcite), radiation damage

## Introduction

The new generation of monochromated and $C_s$-corrected field emission transmission electron microscopes (TEMs) equipped with an energy filter offers high spatial resolution (<1 Å) and the ability to reach an energy resolution below 0.2 eV. This enables acquisition of detailed information about atomic structure, chemical composition, and local electronic states of the investigated object and opens new avenues for quantitative information. One limiting factor for several TEM applications is instability of the samples during electron irradiation and the lack of contrast at medium voltages. Theoretical predictions, as well as experiments, have shown that reduction of the incident electron energy can, in dependence of the material studied, reduce or even avoid the knock-on damage (Egerton, 2012; Meyer et al., 2012). At the same time image contrast and energy resolution improve by reducing the accelerating voltage (e.g., Golla et al., 1994; Reimer, 1997). Calcite ($CaCO_3$) is one of the most abundant minerals in the crust of the earth, is an important system for biomineralization, is one of the main constituents of limestone, and is of enormous importance as an additive in the construction, metallurgical, and chemical industries. When used as material for the construction of buildings, calcite is transformed into CaO by the reaction: $CaCO_3 \rightarrow CaO + CO_2^{\uparrow}$ releasing $CO_2$. It is well known that carbonates are electron beam sensitive (Towe, 1978; Cater & Buseck, 1985; Hofer & Golob, 1987) and apparently the same phase transformation of calcite is initiated in the electron microscope. Walls and Tence (1989) and Murooka and Walls (1991) showed by using a 100 kV VG HB501 and monitoring the change of the electron energy-loss spectroscopy (EELS) spectrum that this transformation is dose rate dependent.

Low dose rates and low accelerating voltages achievable with the sub-Ångström low-voltage transmission electron microscope (SALVE) prototype microscope (Kaiser et al., 2011) are applied to slow down radiation damage effects and give the freedom to align the instrument before beam damage effects can be noticed (Golla-Schindler et al., 2013). This enables monitoring from the start of *in situ* phase transformation and tracking of changes in the chemistry and electronic environment by EELS and electron loss near-edge structure (ELNES).

It is expected that during phase transformation the carbon signal in the EELS spectra will diminish and finally disappear (Walls & Tence, 1989). Additionally the near edge structure of the O-K edge will be significantly changed caused by the loss of the C bondings and the change in the coordination state (Hofer & Golob, 1987). The coordination of the Ca atom in calcite is close to an octahedral coordination if the ligands are aligned along the *x*, *y* and *z*-axis and the octahedron is stretched along the $< 111 >$ direction. The angles between the Ca-O bonds are 87.25 and 92.75° and the bond length is 2.357 Å in all directions (Graf, 1961). In cubic CaO, the calcium atom is octahedral and coordinated

Received December 23, 2013; accepted February 13, 2014
*Corresponding author. ute.golla-schindler@uni-ulm.de

with a bond length between Ca and O atoms of 2.407 Å (Fiquet et al., 1999). Induced by the octahedral coordination of calcium in calcite and CaO the degenerated energy levels of the 3*d* shell split up into $t_{2g}$ and $e_g$ energy levels with an energy difference of $\Delta_o$ (Burns, 1993). The spectrum of the Ca-$L_{2,3}$ edge shows four separated peaks; two are correlated to the transition of Ca $2p_{3/2} \rightarrow 3d$ ($t_{2g}$ $e_g$) and two to this of Ca $2p_{1/2} \rightarrow 3d$ ($t_{2g}$ $e_g$). If, in general, an octahedral site of Ca is distorted along a Cartesian direction, each of the $t_{2g}$ and $e_g$ energy levels split up into two energy levels, one above and one below the original $t_{2g}$, $e_g$ energy levels with an energy difference $\delta$ (Burns, 1993). If then core shell electrons are excited in all present energy levels and the energy resolution and detection limit are sufficient, we expect the EELS spectrum to show eight separated peaks with shifted peak positions above and below the peak position for the undistorted octahedral coordination. In this paper we investigate transition from calcite to CaO in the microscope at 80, 40, and 20 kV, and observe *in situ* the symmetry and bond length changes via ELNES.

## Materials and Methods

The starting material for the TEM studies was a clear natural calcite rock from Brilon (Germany). Small crystal fragments thin enough for TEM investigations were produced by crushing liquid nitrogen cooled small pieces of the original calcite rock. They were separated in an ultrasonic bath and supported on lacey-carbon films. Calcite ($CaCO_3$) is a carbonate mineral, trigonal-rhombohedral with the space group R3 2/*c* and $a = 4.9899$ Å, $c = 17.064$ at 26°C (Graf, 1961), where the Ca atom is six-fold coordinated and C and O atoms are three-fold coordinated. $CaCO_3$ decarbonates in the TEM to CaO by releasing $CO_2$. The crystal system of CaO is cubic with the space group Fm-3m, and a lattice constant of a = 4.81 Å where Ca and O are octahedral coordinated (Fiquet et al., 1999).

The studies were performed with the SALVE I prototype microscope. This microscope is dedicated for low kV applications and was aligned for accelerating voltages of 80, 40, and 20 kV. It is equipped with a Schottky field-emission gun, the CEOS electrostatic Omega-type monochromator (Kahl & Rose, 2000; Uhlemann & Haider, 2002), an in-column energy filter of the corrected OMEGA type (Lanio et al., 1986), a CEOS image-side $C_s$-corrector (Rose 1990, Uhlemann et al., 1994) and a 4kx4k CMOS TVIPS camera F416 (Tietz et al., 2012). Instrument alignment, image and spectra acquisition were performed with *WinTEM*, *ZEMAS* (Zeiss), Tietz, and CEOS software. The image and EELS data processing was performed by using *Digital Micrograph* (Gatan), *JEMS* (Piere Stadelmann), and *Igor* (Wave Metrics) software.

To obtain experimental data, measuring cycles of images and spectra were recorded during the electron beam-induced phase transformation. In each cycle, first a zero-loss filtered and an unfiltered image were acquired. Then the operation mode was switched to the spectroscopy mode and EELS spectra for the C-K, Ca-L, and O-K edges were recorded. Afterwards, the operation mode was switched back to image mode and the next cycle was started. The images were used to control and keep the specimen position constant and to calculate $t/\lambda_i$ maps to determine possible thickness reduction. Knowledge of particle size and thickness reduction offers the opportunity to quantify volume loss induced by radiation damage (Golla-Schindler et al., 2013).

All series at 80, 40, and 20 kV accelerating voltages were taken with magnifications above 300 k to control the unaltered crystal structure at the beginning by imaging lattice planes. An energy filter slit width corresponding to 1–2 eV was used to acquire images containing solely elastically scattered electrons for calculation of the $t/\lambda_i$ maps. To enable the comparison of images and spectra as a function of accelerating voltage, similar dose rates were adjusted for all voltages by the condensor zoom. About the same energy resolutions were adjusted by choosing a suitable monochromator slit width in the range of 1–2 $\mu$m. To obtain the dose rates, in the first step the conversion rate of the CMOS camera was measured for all accelerating voltages used. Then, in each experiment, an additional image of a specimen-free area was taken without changing the imaging conditions. This offers the opportunity to obtain the dose rate simply by converting count rates into dose rates. The series were taken with dose rates of $4.1 \times 10^4$, $3.4 \times 10^4$, and $3.1 \times 10^4$ e/nm$^2$ s for 80, 40, and 20 kV, respectively. Energy resolutions were determined by the full width at half maximum of the zero-loss peak and were 0.32, 0.29, and 0.23 eV for 80, 40, and 20 kV experiments, respectively. The image area for the spectroscopy part was selected by using a spectrometer entrance aperture, which just fits to the field of view on the CMOS camera. All spectra were recorded with the CMOS camera with dark and flat-field correction. The ELNES peak positions were determined by using *Igor* and the incorporated peak-fitting routine.

## Results and Discussion

Characteristic images of an experiment performed at 20 kV with a dose rate of $4.0 \times 10^4$ e/nm$^2$ s are shown in Figure 1. As depicted, electron beam-induced phase transformation occurred: First the amorphization of the crystalline structure, then the production of holes, and finally recrystallization in a polycrystalline structure. Figure 1a presents the first image of the experiment, where the lattice planes of calcite can be imaged without noticeable electron beam-induced degradation effects. This confirms the single crystalline structure of the initial material. In the correlated Fast Fourier Transformation (FFT) (Fig. 1b) the lattice plane distance shown is 3.86 Å, which fits with theoretical predictions of 3.87 Å for the (012) lattice plane of calcite performed with JEMS, and the crystallographic data of Graf (1961). After 6 min of permanent electron irradiation, the image illustrated in Figure 1c was taken. The (012) lattice planes of the calcite structure are still partially present, but the beginning of the phase transformation is now clearly visible by the

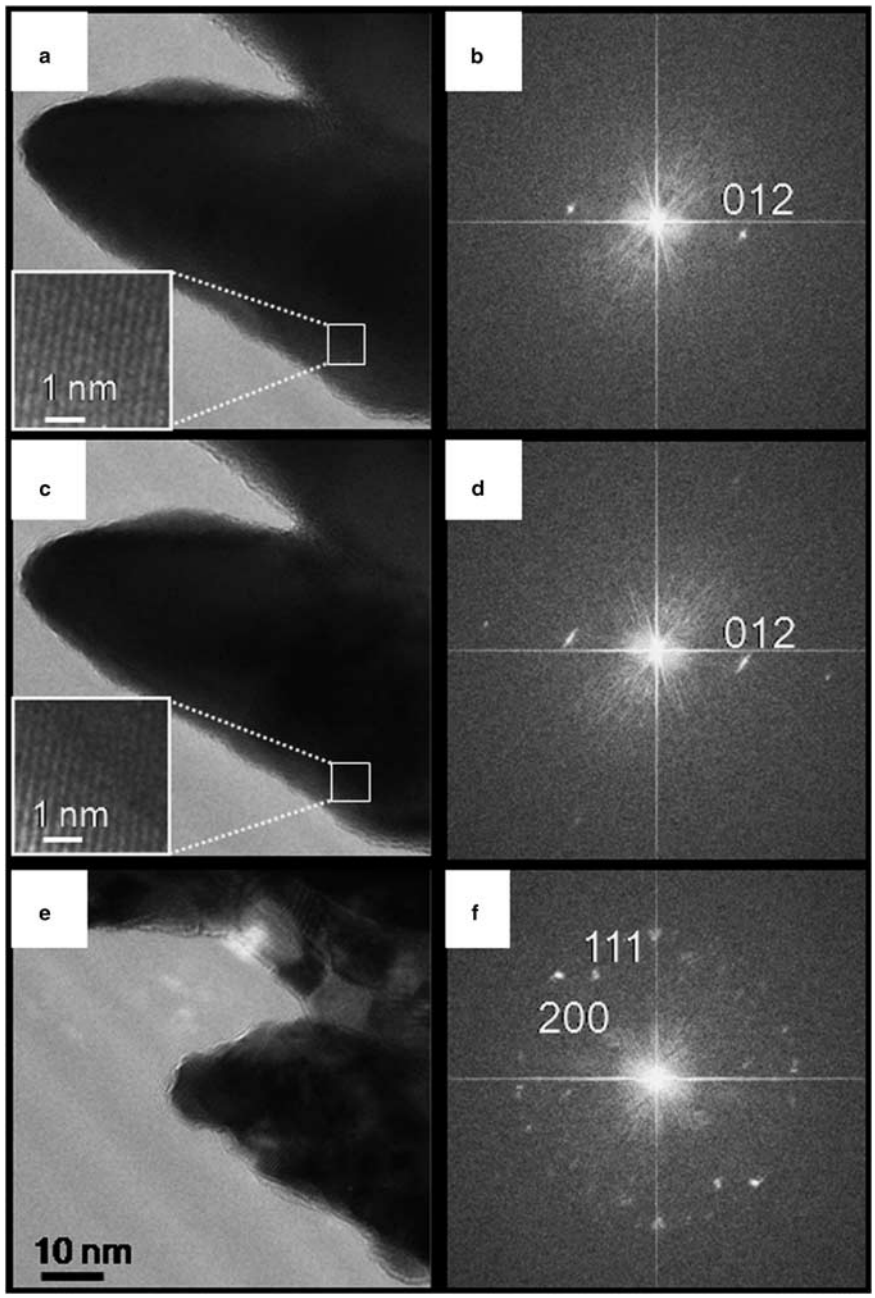


**Figure 1.** 20 kV high-resolution TEM (HRTEM) images and their corresponding FFTs visualizing different stages of the phase transformation of calcite to CaO. **a**, **b:** In the initially single-crystalline calcite structure (**c**, **d**) amorphous regions begin to form**. e**, **f**: After further irradiation, the polycrystalline CaO structure has been formed identified by the 111 and 200 spots in the corresponding FFT.

production of bent lattice planes and amorphous regions. This leads to blurred and elongated diffraction spots in the corresponding FFT (Fig. 1d). The same phenomenon can be found in the field of mineralogy when handling materials containing impurities of radioactive compounds and is called the metamictization process (Klein & Hurlbut, 1993).

Figure 1e shows the same crystal after 25 min of electron irradiation and as can be seen, the shape of the irradiated particle has been changed. Moreover, it now presents a polycrystalline structure (see the corresponding FFT Fig. 1f) and the volume is significantly diminished (see Fig. 1e). In the corresponding FFT (Fig. 1f) rings of randomly distributed diffraction spots appear, which confirm the polycrystalline nature. The ring radii were determined to be $2.39 \pm 0.02$ and $2.76 \pm 0.02$ Å, which fit with theoretically calculated reflections for the (200) 2.40 Å and (111) 2.77 Å lattice planes of CaO using the crystallographic data of Fiquet et al. (1999) and JEMS.

Such phase transformation induced by electron irradiation has previously been studied on the same or similar

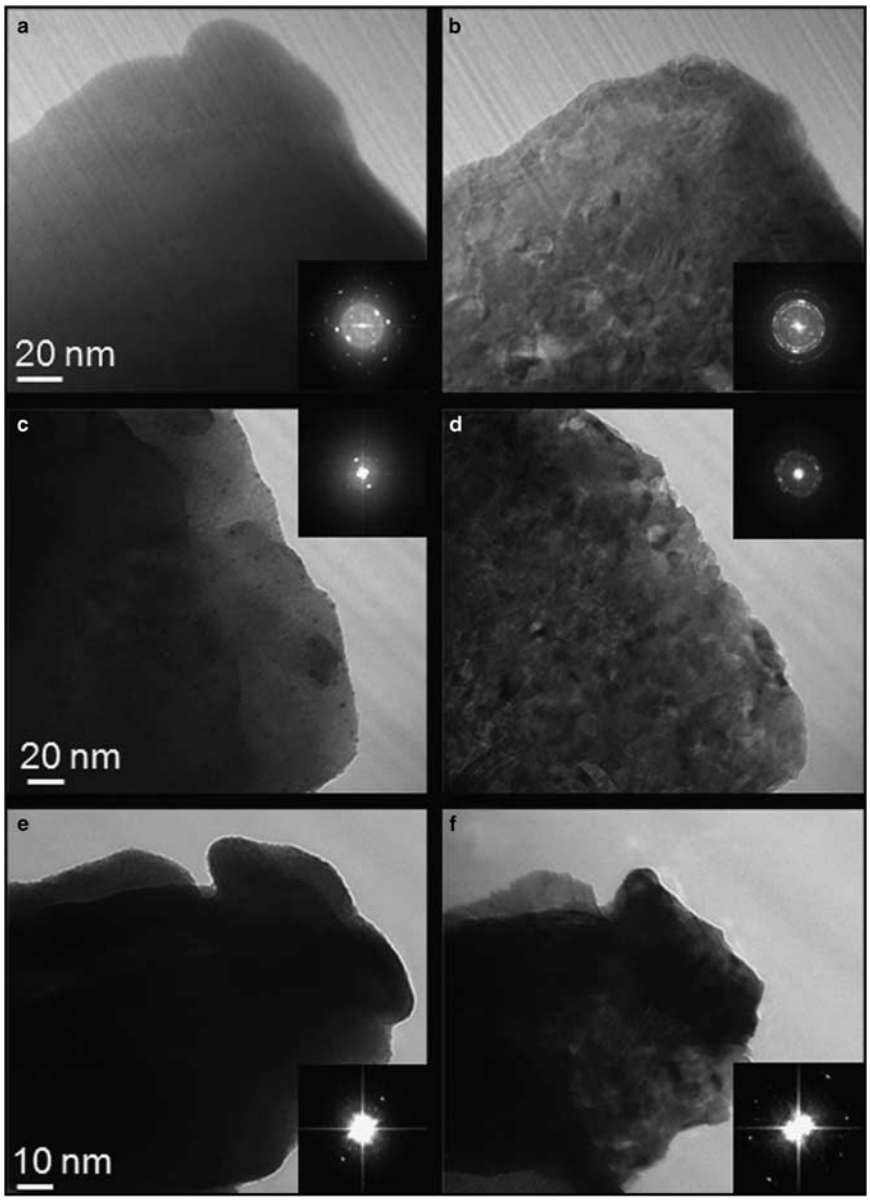


**Figure 2.** 80 kV (**a**, **b**), 40 kV (**c**, **d**) and 20 kV (**e**, **f**) high-resolution TEM (HRTEM) images related to the phase transformation experiment shown in Figures 3–5. The insets show the corresponding FFTs.

systems like dolomite by high-resolution TEM and diffraction analysis using accelerating voltages from 100 up to 120 kV (Towe, 1978; Cater & Buseck, 1985; MkHoyan et al., 2006). Our observation showed that this transformation can be initiated at much lower accelerating voltages of 80, 40, and 20 kV by using dose rates of ~$4 \times 10^4$ e/nm$^2$ s. Figure 2 illustrates the first and last images of the experiments at 80 kV (Figs. 2a, 2b), 40 kV (Figs. 2c, 2d), and 20 kV (Figs. 2e and 2f), which were chosen for the ELNES studies. The inserted FFTs confirm the single and polycrystalline structure of the initial and end material, respectively. It can be seen in the insert in Figure 2a that at 80 kV the initial image is not single crystalline any more. We interpret this as we were not fast enough and the transformation had already started. The samples used for the 80 and 40 kV studies were covered with gold nanoparticles (dark dots) for further contrast studies in another project.

Characteristic EELS spectra of the 80 kV experiment are shown in Figure 3, where a, b, and c are the C-K, the Ca-$L_{2,3}$, and the O-K edges, respectively. The lowest red spectra of the C-K, the Ca-$L_{2,3}$ and the O-K EELS spectra all belong to the first measurement cycle and the following black to the second, and so on. The experiment was run for more than 90 min and the spectra are all raw data without noise reduction or energy drift correction. This demonstrates the high stability of the instrument. Only the astigmatism and the specimen position had to be slightly realigned from time to time. Figure 3a presents changes in the C-K edge ELNES of the 80 kV experiment. Here, the fine structure of the C-K edge of the initial state is different than amorphous carbon and shows a sharp peak positioned at 288.4 eV, followed by less intense broader peaks, a small peak at 293.4 eV, and the second highest broader peak at 299.8 eV, with a shoulder

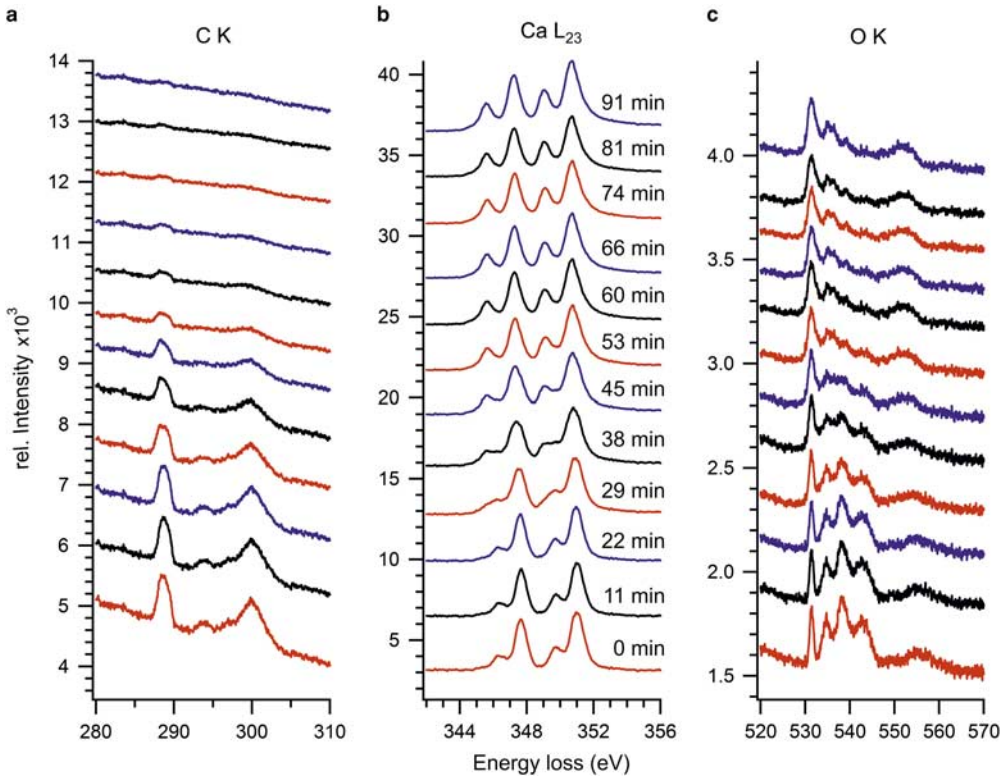


**Figure 3.** 80 kV electron energy-loss spectroscopy (EELS) spectra for time-dependent changes of (**a**) C-K, (**b**) Ca-$L_{2,3}$ and (**c**) O-K edges (the experiment time is assigned in (**b**)). The curves presented on the same *y*-axis level with the identical color belong to one measurement cycle.

at 296.9 eV. This ELNES is characteristic for carbonates, or accordingly the complex ion $CO_3^{2-}$ (Hofer & Golob, 1987; Garvie et al., 1994). Hofer and Golob (1987) solely resolved two peaks at 289 and 300 eV in their studies on calcite and dolomite, where the peak positions as well as the peak shape fits with the ELNES recorded in our experiments. The signal of the carbon edge decreased over time until it completely vanished. This is expected due to the decarbonization until only pure CaO remains. In Figure 3b, the ELNES of the Ca-$L_{2,3}$ edge is illustrated, where four peaks can be separated: the first two are correlated to the Ca $2p_{3/2} \rightarrow 3d$ ($t_{2g}$ $e_g$) and the second two to the Ca $2p_{1/2} \rightarrow 3d$ ($t_{2g}$ $e_g$) transitions. During the phase transformation a peak shift of all peaks as well as a change in the peak distance of the $L_{2,3}$ ($t_{2g}$ $e_g$) peak positions is obvious (further details see Figs. 4 and 5).

Figure 3c presents the change in the O-K edge ELNES during the phase transformation, where the starting spectrum of calcite shows four relatively sharp peaks in the range of 10 eV and a smooth one around 25 eV above the edge onset. The first peak at 531.4 eV is preserved during the phase transformation, where the following peaks are significantly reduced and change their positions. The second and third peak at 534.7 and 538.1 eV are broadened and diminish with time while the peak positions change to 535.4 and 539.3 eV, respectively. The fourth sharp peak at 543.7 vanishes completely. The smooth peak at around 555 eV shifts to ~552 eV. It was suggested by de Groot et al. (1989) and Krivanek and Paterson (1990) for metal oxides that the sharp structures of the O-K edge within 5 eV of the edge threshold can be assigned to hybridization of the oxygen 2*p* and metal 3*d* energy levels. The second region above 5 eV of the edge onset is assigned to hybridization of the oxygen 2*p* and metal 4*s* levels. In our case, ELNES of the O-K edge is a superposition of the hybridization of oxygen with calcium and carbon. The hybridization of the Ca atom is conserved during the phase transformation, which fits to the preservation of the first peak. This can be assigned to hybridization of the oxygen 2*p* with the Ca 3*d* energy levels. Induced by decarbonization during the phase transformation, hybridization with carbon is finally lost and the amount of oxygen is reduced. This causes the significant changes of the O-K edge ELNES. Finally, the oxygen near edges shows characteristics expected for CaO (Hofer & Golob, 1987).

Figure 4 presents the ELNES of the Ca $L_{2,3}$ edge for the 40 kV (Fig. 4a) and 20 kV (Fig. 4b) series. These four peaks can be separated, with two of them correlated to the Ca $2p_{3/2} \rightarrow 3d$ ($t_{2g}$ $e_g$) and two of them to the Ca $2p_{1/2} \rightarrow 3d$ ($t_{2g}$ $e_g$) transitions. Examples for the 20 kV measurements and determined peak positions are listed in Table 1. For 40 and 20 kV, we obtained starting peak positions of the Ca-$L_{2,3}$ edges-characteristic for calcite, indicated by blue dashed lines. The second end peak-position-characteristic for CaO is indicated by red dashed lines. In the middle of the phase transformation a superposition of the starting and end

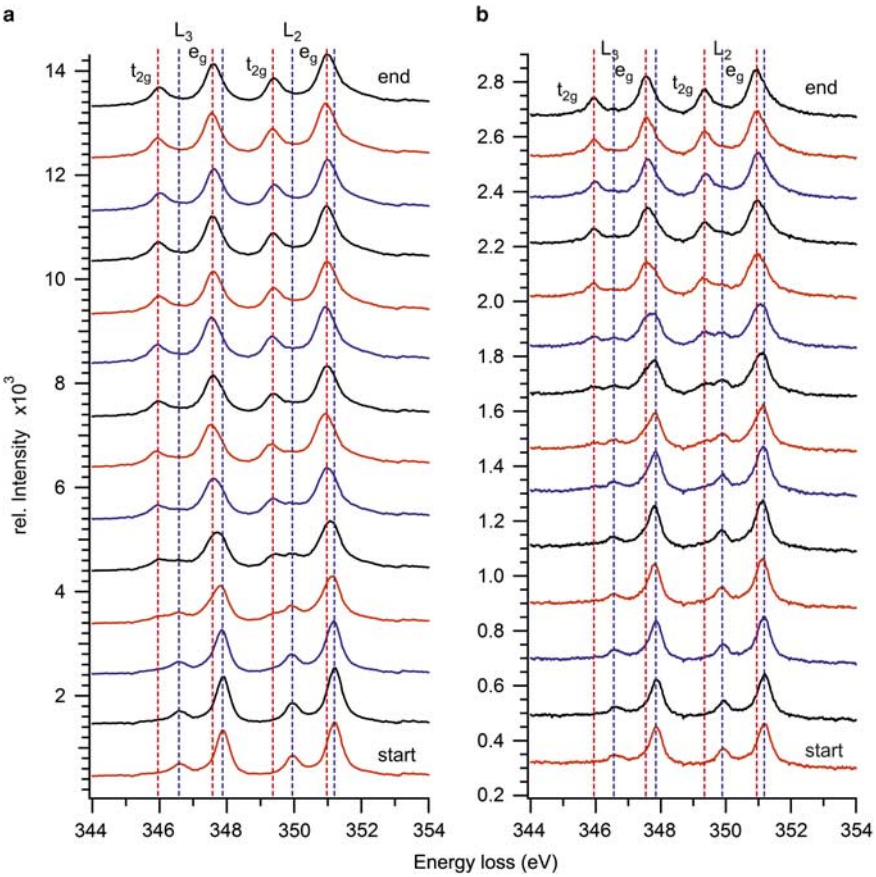


**Figure 4.** 40 kV (**a**) and 20 kV (**b**) electron loss near-edge structure (ELNES) of the time-dependent changes of the Ca-$L_{2,3}$ edge assigned to the phase transformation experiment shown in Figure 2c–2f. The blue dashed lines are aligned to the peak position of the $CaO_3$ ELNES and the red dashed lines to the peak positions of CaO ELNES.

spectra with resolved peak positions is detectable. Solely, these two peak positions exist in all spectra (see also Fig. 5). This proved that the change in the peak position cannot be initiated by energy drift of the experimental setup, but is caused by change in the electronic environment of the Ca atom. Figures 5a and 5b presents the start, middle and end spectra of the Ca $L_{2,3}$ edge of the 40 and 20 kV experiment, where the red curves show the spectra at the beginning, the blue curves at the middle, and the black curves at the end of the phase transformation. The comparison of these curves show the changes in the Ca $L_{2,3}$ $t_{2g}$ and $e_g$ peak positions. All peaks shift to lower energies and additionally the energy level splitting $\Delta_o$ increases. The middle spectra clearly show superposition of the ELNES characteristics of calcite and CaO. The 20 kV series shows a more pronounced peak separation of the Ca-$L_{2,3}$ $t_{2g}$ peak positions for calcite and CaO than the 40 kV series. This improvement can be addressed to the increase in energy resolution for reduced accelerating voltages.

During the phase transformation of calcite to CaO, octahedral coordination of calcium with oxygen as a binding partner is preserved, but the distortion is removed and the bond length changes from 2.357 Å ($CaCO_3$) to 2.407 Å (CaO) by 5 pm. Both changes can be the reason for alteration of the calcium ELNES. Muller (1999) showed that changes in bond lengths for Ni-Al and Ni-Si compounds generate core level shifts, where the sign of the core level shift changes with filling of the 3*d* states. The energy levels shift to lower energies for less than half filled 3*d* states. Furthermore, he found for Ni a core level shift of ≈2 eV for a bond length change of 0.5 Å. His findings agree with our results, because calcium has less than half-filled 3*d* states and all peaks of the Ca-$L_{2,3}$ edge shift to lower energies. The calculated energy shifts of the Ca-$L_{2,3}$ $e_g$ peak position are listed in Table 2. In comparison with Muller (1999), we yield the same relationship, but the energy level shift as well as the bond length variation are much smaller, and reduced by approximately a factor of 10.

Due to the octahedral coordination of calcium, the 3*d* shell splits up into the $t_{2g}$ and $e_g$ energy levels and the lobes of the atomic orbital for the $t_{2g}$ energy levels project between the cartesian axes, and the lobes of the atomic orbital of the $e_g$ energy levels are directed along the cartesian axes. Therefore it can be expected that changes in the bond length will significantly influence the $t_{2g}$ and $e_g$ energy levels in a different way and will change $\Delta_o$. In Burns (1993) the dependence of $\Delta_o$ on bond length changes was discussed, where he predicted that a decrease in the bond length of the

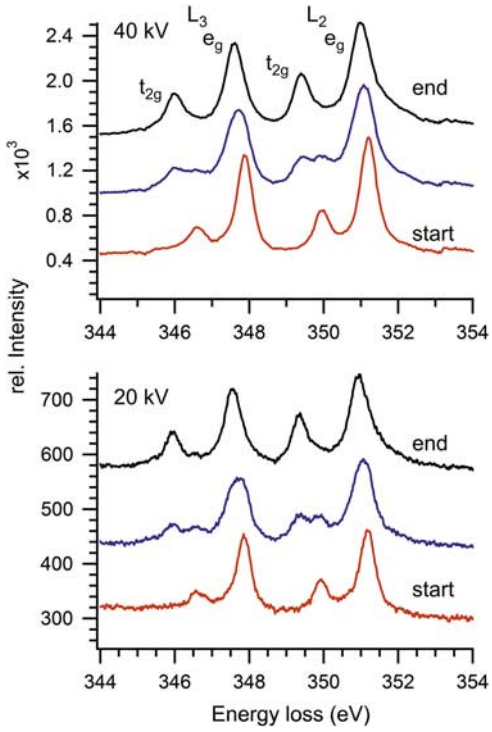


**Figure 5.** 40 kV (**a**) and 20 kV (**b**) Ca-$L_{2,3}$ edge electron loss near-edge structure (ELNES) showing only the start (red), the middle (blue), and the finish (black) of the phase transformation of Figure 4 for better visibility of the differences.

crystal structure would lead to a decrease in $\Delta_o$ in the crystal field spectra. This is demonstrated with experimental results for the replacement of $Mg^{2+}$ ions by $Fe^{2+}$ ions in olivin.

Changes in symmetry can also significantly change the ELNES. Rez and Blackwell (2011) studied calcite, aragonite, and the amorphous phase of calcium carbonates. Their experimental spectra showed an unchanged peak position for the $L_{2,3}$-$e_g$ edges, but a change in the peak shape and position for the $L_{2,3}$-$t_{2g}$ edges for the different calcium carbonates. Their theoretically fitted EELS spectra performed with multiplet calculation using the CTM4 × 4S code suggest that a change of symmetry and distortion introduce a change in the ELNES. It is known from Burns (1993) that for tetragonal distorted octahedral sites along one Cartesian axis, the $t_{2g}$ and $e_g$ energy levels each split up into two further energy levels, one above and one below the original $t_{2g}$ and $e_g$ energy levels. If then core shell electrons are excited in all present energy levels, and the energy resolution and detection limit is sufficient, supplementary peaks in the EELS spectrum should appear. For each original $t_{2g}$ and $e_g$ peak two peaks should appear, with one peak with increased energy and one with decreased energy in relation to the original peak position of the $t_{2g}$ and $e_g$ peak position. This does not agree with our finding. Alternatively, when mostly transitions to the lower energy levels are excited, $\Delta_o$ decreases in comparison with the undistorted state. That means that $\Delta_o$, should increase during the phase transformation from calcite to CaO, which agrees with our results. Additionally the peak positions of all Ca-$L_{2,3}$ edges should shift to higher energies for the undistorted state, in our case CaO, which is contrary to our results. The distortion in calcite is not along a Cartesian axis, and therefore this may introduce deviant effects in the ELNES.

**Table 1.** Ca $L_{2,3}$ Edge Peak Positions for the First and Last Spectra of the 20 kV Experiment.

| | 20 kV (start) | 20 kV (end) |
|---|---|---|
| Ca $L_3$ $t_{2g}$ | 346.52 eV | 345.94 eV |
| Ca $L_3$ $e_g$ | 347.86 eV | 347.56 eV |
| Ca $L_2$ $t_{2g}$ | 349.91 eV | 349.34 eV |
| Ca $L_2$ $e_g$ | 351.21 eV | 350.94 eV |

**Table 2.** Caculated Energy Shift Values of the Ca $L_3$ $e_g$ and Ca $L_2$ $e_g$ Peak Positions Displayed in Figure 5.

| | 40 kV | 20 kV |
|---|---|---|
| Shift $L_3$ $e_g$ | 268 meV | 304 meV |
| Shift $L_2$ $e_g$ | 215 meV | 262 meV |

## Summary and Conclusion

Operating the SALVE I prototype microscope at 20 and 40 kV we were able to yield an energy drift stability, sufficient to track *in situ* the phase transformation from $CaCO_3$ to CaO which took more than 1 h under our conditions. This electron beam-induced phase transformation occurs in different stages: first an amorphization of the crystalline calcite takes place, followed by production of holes, and finally the recrystallization into a polycrystalline structure. We showed that this transformation can be initiated at 80, 40, and 20 kV. At 80 kV, images and the correlated EELS results indicate that the phase transformation has partially started right from the start of the experiment. The highest-resolved ELNES results for the Ca-$L_{2,3}$ edge are delivered by using an accelerating voltage of 20 kV where the superposition of the calcite and CaO ELNES is clearly visible. The initial C-K and O-K edge ELNES deliver the peak shapes and peak positions characteristic for calcite. Caused by the decarbonization, the C-K edge diminishes and disappears during the phase transformation. The oxygen near edge structure changes from a structure characteristic of calcite to those of CaO. The Ca ELNES presents four separated peaks for calcite and CaO. A shift of all Ca $L_{2,3}$ peak positions to lower energies and an increase in the energy level splitting $\Delta_o$ is experimentally detected. The shift of the peak positions to lower energy losses agrees with findings of Muller (1999) for materials with less than half filled 3*d* states. However, bond length changes as well as symmetry changes could potentially introduce the observed increase of the splitting of the energy levels during the phase transformation.

Future work will address these questions by simulations of the ELNES structure for both of the cases.

## Acknowledgments

This work was supported by the D.F.G. (German Research Foundation) and the Ministry of Science, Research and the Arts (M.W.K.) of Baden-Wuerttemberg in the frame of the SALVE (Sub Angstrom Low-Voltage Electron microscopy and spectroscopy project. We thank the Institute of Mineralogy Münster (Prof. Dr. P. Schmid Beurmann) for the samples and S. Groezinger for the sample preparation.

## References

Burns, R.G. (1993). *Mineralogical Applications of Crystal Field Theory*. Cambridge, New York: Cambridge University Press. pp. 30–36.

Cater, D.E. & Buseck, P.R. (1985). Mechanism of decomposition of dolomite $Ca_{0.5}Mg_{0.5}CO_3$, in the electron microscope. *Ultramicroscopy* **18**, 241–252.

deGroot, F.M.F., Grioni, M. & Fuggle, J.C. (1989). Oxygen 1*s* x-ray-absorption edges of transition-metal oxides. *Phys Rev B* **40**, 5715–5723.

Egerton, R.F. (2012). Mechanism of radiation damage in beam-sensitive specimens, for TEM accelerating voltages between 10 kV and 300 kV. *Microsc Res Tech* **75**, 1550–1556.

Fiquet, G., Richet, P. & Montagnac, G. (1999). High-temperature thermal expansion of lime, periclase, corundum and spinel. *Phys Chem Minerals* **27**, 103–111.

Garvie, L.A.J., Craven, A.J. & Brydson, R. (1994). Use of electron-energy loss near-edge fine structure in the study of minerals. *Am Mineralogist* **79**, 411–425.

Golla, U., Schindler, B. & Reimer, L. (1994). Contrast in the transmission mode of a low-voltage scanning electron microscope. *J Microsc* **173**, 219–225.

Golla-Schindler, U., Schweigert, W., Benner, G., Orchowski, A. & Kaiser, U. (2013). Quantitative study of electron radiation damage by *in situ* observation of the phase transformation from $CaCO_3$ to CaO with high and Low kV transmission electron microscopy. *Microsc Microanal* **19**(Suppl 2), 1214–1215.

Graf, D.L. (1961). Crystallographic tables for the rhombohedral carbonates. *Am Mineralogist* **46**, 1283–1316.

Hofer, F. & Golob, P. (1987). New examples for near-edge fine structures in electron energy loss spectroscopy. *Ultramicroscopy* **21**, 379–384.

Kahl, F. & Rose, H. (2000). Design of a monochromator for electron sources. *Proc 11th Eur Cong Electr Micr* **1**, 1459–1460.

Kaiser, U., Biskupek, J., Meyer, J.C., Leschner, J., Lechner, L., Rose, H., Stoger-Pollach, M., Khlobystov, A.N., Hartel, P., Muller, H., Haider, M., Eyhusen, S. & Benner, G. (2011). Transmission electron microscopy at 20 kV for imaging and spectroscopy. *Ultramicroscopy* **111**, 1239–1246.

Klein, C. & Hurlbut, C.S. Jr. (1993). Metamict minerals. In *Manual of Mineralogy (after James D. Dana)*, 21st ed. Klein C. & Hurlbut C.S. Jr (Eds.), pp. 159–160. New York: Wiley.

Krivanek, O.L. & Paterson, J.H. (1990). ELNES of 3d transition-metal oxides. *Ultramicroscopy* **32**, 313–318.

Lanio, S., Rose, H. & Krahl, D. (1986). Test and improvement design of a corrected imaging magnetic energy filter. *Optik* **73**, 56–68.

Meyer, J.C., Eder, F., Kurasch, S., Skakalova, V., Kotakoski, J., Park, H.-J., Roth, S., Chuvilin, A., Eyhusen, S., Benner, G., Krasheninnikov, A.V. & Kaiser, U. (2012). Accurate measurement of electron beam induced displacement cross sections for single-layer graphene. *Phys Rev Lett* **108**, 196102–196108.

MkHoyan, K.A., Silcox, J., McGuire, M.A. & Disalvo, F.J. (2006). Radiolytic purification of CaO by electron beams. *Philosophical Mag* **86**, 2907–2917.

Muller, D. (1999). Why changes in bond length and cohesion lead to core-level shifts in metals, and consequences for the spatial difference method. *Ultramicroscopy* **78**, 163–174.

Murooka, Y. & Walls, M.G. (1991). Beam damage on anisotropic material ($CaCO_3$) in STEM. EMAG 91. *Inst Phys Conf Ser* **119**, 337–340.

Reimer, L. (1997). *Transmission Electron Microscopy*, 4th ed. Berlin, Heidelberg, New York: Springer Verlag.

Rez, P. & Blackwell, A. (2011). Ca $L_{23}$ spectrum in amorphous and crystalline phases of calcium carbonate. *J Phys Chem B* **115**, 11193–11198.

Rose, H. (1990). Outline of a spherically corrected semi-aplanatic medium-voltage TEM. *Optik* **85**, 19–24.

Tietz, H., Ghadimi, R. & Daberkow, I. (2012). Single electron events in TEM. *Imag Microsc* **14**, 46–48.

Towe, K.M. (1978). Ultrastructure of clacite decomposition in vacuo. *Nature* **274**, 239– 240.

Uhlemann, S., Haider, M. & Rose, H. (1994). Procedures for adjusting and controlling the alignment of a spherically corrected electron microscope. In *ProcICEM-13 Paris*, B. Jouffrey (Ed.), *et al.*, pp. 193–194. Paris I: Les Editions de Physique.

Uhlemann, S. & Haider, M. (2002). Experimental set-up of a fully electrostatic monochromator for a 200 kV TEM. *Proc 15th Int Cong Electr Micr* **3**, 327–328.

Walls, M.G. & Tence, M. (1989). EELS study of beam-induced decomposition of calcite in STEM. EMAG-MICRO 89. *Inst Phys Conf Ser* **98**, 255–258.